Desalination and Water Treatment
www.deswater.com

doi:10.5004/dwt.2019.24444

164 (2019) 319–325
October

Facile fabrication of Ag_3PO_4/chitosan membrane composite with visible light photo catalytic performance

Geng Li[a,b,c,*]

[a]*NARI Group Corporation Ltd. Nanjing 211106, China, e-mail: ligeng306@163.com (G. Li)*
[b]*Wuhan NARI Limited Liability Company, State Grid Electric Power Research Institute, Wuhan 430074, China,*
[c]*Hubei Key Laboratory of Power Grid Lightning Risk Prevention, Wuhan 430074, China*

Received 2 February 2019; Accepted 20 May 2019

ABSTRACT

In this work, Ag_3PO_4/chitosan membrane composites were prepared by a facile method of in-situ synthesis. The structure and properties of the obtained Ag_3PO_4/chitosan membrane composites were characterized using scanning electron microscopy, Fourier transform infrared spectroscopy, X-ray diffraction, X-ray photo electron spectroscopy, and ultraviolet-visible diffuse reflection absorptive spectra. Photo catalytic properties were investigated via degradation of a methyl orange solution under visible light irradiation. Decolorization results indicated that the decolorization efficiency of Ag_3PO_4/chitosan membrane composites were better than that of pure Ag_3PO_4 particles. The impacts of different concentrations of $AgNO_3$ solutions (0.1, 0.2, and 0.3 mol/L) in the experimental process were discussed. At concentrations of 0.2 mol/L, the composite exhibited much higher photo catalytic activity performance under visible light irradiation.

Keywords: In-situ synthesis; Ag_3PO_4; Chitosan membrane; Photo catalytic performance

1. Introduction

Over the past few decades, dye effluents have become one of the main sources of water pollution [1]. Photo catalytic degradation technology, as one of the most environmentally sound technologies, has attracted substantial attention in the removal of various dye pollutants and hydrogen evolution [2]. Several photo catalysts have been synthesized, such as $CsPbBr_{3-x}I_x$ [3], $Ag/AgCl/TiO_2$ [4], Ag_2ZnSnS_4/Mo [5] and Ag-ZnO [6]. In the last 10 years, numerous studies have reported that multifarious silver-based semiconductor photo catalysts possess several advantages including significant visible and UV photo catalytic properties [7–10]. Among these semiconductors, silver phosphate (Ag_3PO_4) is an efficient photo catalyst with an indirect band gap of 2.36 eV as well as a direct transition of 2.43 eV; its excellent degradation of organic dyes and strong photo oxidative capacity for O_2 evolution under visible light irradiation with quantum efficiency up to 90% was first reported by Ye et al. [11]. However, the application of single-phase Ag_3PO_4 remains constrained by inherent drawbacks including high cost, low photo stability, large particle size with smaller surface area, and tendency to agglomerate, leading to decreases in surface area and surface energy [12,13]. To overcome these problems, Ag_3PO_4 nanoparticles have been coupled with CeO_2 [14], $BiVO_4$ [15], Ag_2S [16], MoS_2 [17], and g-C_3N_4 [18] to reduce agglomeration of Ag_3PO_4 nanoparticles. Another problem is that nanoparticles are difficult to remove from solutions; some researchers have immobilized Ag_3PO_4 particles on PAN nanofibers [19], sulfonated polyphenylene sulfide superfine fiber [20], and cellulose [21] to promote easy recyclability.

Chitosan, a widespread semi-natural polysaccharide, is non-toxic, inexpensive, hydrophilic, biocompatible, biodegradable, and anti-bacterial [22], arousing great interest in various fields [23]. Due to the presence of abundant hydroxyl (-OH) and a mine ($-NH_2$) groups that can serve as active sites for the adsorption of other organic compounds as well as metal ions including Hg^{2+}, Cd^{2+}, Zn^{2+}, Cu^{2+}, Ni^{2+}, and Ag^+ [24,25], chitosan has been researched extensively as a base material for analytical (e.g., separation, chromatogra-

*Corresponding author.

phy, biosensor, affinity, and fluorescence probes), biomedical (e.g., enzyme-based biofuel cells, bone regeneration, anti-cancer embolotherapy, and targeted drug carriers), and environmental (e.g., pollutant removal and toxic pollutant degradation) applications [26].

In this paper, we use a chitosan membrane as an adsorbent and soft template to immobilize Ag_3PO_4. Ag_3PO_4 particles can be easily anchored onto the chitosan membrane by in-situ polymerization, and the photo catalytic performance of as-prepared Ag_3PO_4/chitosan membranes under visible light irradiation is evaluated by photo degradation of a methyl orange (MO) solution. The photo catalytic effects of different concentrations of Ag^+ ions chelating with chitosan membranes are investigated.

2. Experiment

2.1. Materials

Chitosan was provided by Shanghai Macklin Biochemical Co., Ltd. (Viscosityt, 200–400 mPa·s; degree of deacetylation: 95%). Silver nitrate ($AgNO_3$) and disodium hydrogen phosphate (Na_2HPO_4) were purchased from Sinopharm Chemical Reagent Corp (PR China).

2.2. Preparation of chitosan porous membranes

Chitosan porous membranes were prepared by casting an acid chitosan solution (1.5%, w/w, of chitosan–5% acetic acid solution) on Petri dishes. Dishes were kept at 60°C for 2 h until the mass became constant. Membranes were then immersed for 12 h in 1 mol/L NaOH solution at room temperature to neutralize excess acid [27]. Afterwards, they were washed thoroughly with distilled water and stored in water at 4°C.

2.3. Preparation of Ag_3PO_4/chitosan membrane composites

0.1 g as-prepared chitosan membranes were immersed in 50 ml $AgNO_3$ solution at different concentrations (0.1, 0.2, and 0.3 mol/L) for 5 h to allow chelation of Ag^+ ions with a mine groups. Then, 50 ml 0.2 mol/L Na_2HPO_4 was added into the above solution drop by drop. The reaction was maintained with continuous shaking for 3 h, and each treated sample was thoroughly rinsed with distilled water followed by drying at 60°C for 3 h. The Ag_3PO_4/chitosan membrane composites were marked as composite-1, composite-2, and composite-3, obtained through treatment with 0.1 mol/L, 0.2 mol/L, and 0.3 mol/L of $AgNO_3$ solutions, respectively. A schematic illustration of the growth process of Ag_3PO_4 on the chitosan membrane is provided in Fig. 1.

2.4. Characterization

The size and micro morphology of the chitosan membrane and Ag_3PO_4/chitosan membrane composites were observed with a JSM-IT300A scanning electron microscope (SEM). The surface functionalization and bonding configuration of all samples were determined by VERTEX 70 Fourier transform infrared spectroscopy (FTIR) ranging from 450 to 4000 cm^{-1}. Crystal patterns of samples were characterized by a Rigaku MiniFlex 600 X-ray diffractometer (XRD) with a Cu Kα target at 40 kV and 40 mA at a scan rate of 5°/min from 10° to 80° (2θ). Elemental analysis of composite-2 was conducted by AXIS-ULTRA DLD-600W X-ray photo electron spectroscopy (XPS). Light absorption of the samples was measured by ultraviolet-visible diffuse reflection absorptive spectra (UV–vis/DRS) with a UV-2700 UV-visible spectrophotometer.

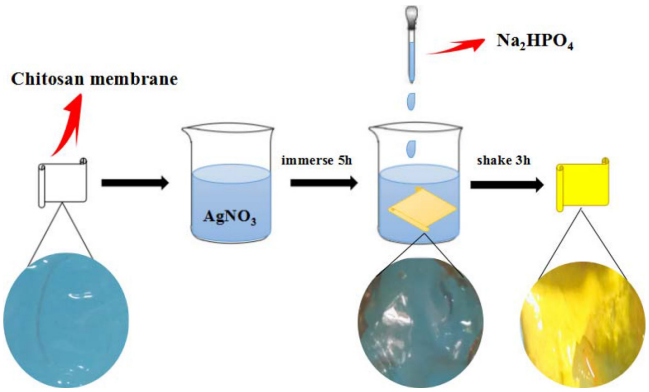

Fig. 1. Schematic illustration of the growth process of Ag_3PO_4 on chitosan membrane.

2.5. Photo catalytic activity measurement

Photo catalytic activity of Ag_3PO_4/chitosan membrane composites was evaluated by the ability to decompose an MO solution (100 ml, 10 mg/L) under visible light irradiation. The initial pH of the MO solution was adjusted to pH 7.0. Typically, 0.1 g Ag_3PO_4/chitosan membrane composite was added to the MO solution and magnetically stirred for 10 min under dark conditions to establish the adsorption/desorption equilibrium. Then, the suspension was irradiated with a 300 W Xe arc lamp. At 4-min intervals, approximately 4 ml of the suspension was collected. Obtained clear solutions were recorded at 464 nm (λ_{max} for MO solution) by UV–vis spectrometry, and the obtained values were used to calculate the decoloriation rate of the MO dye solutions.

The decolorization rate of the MO dye solutions was calculated with the following equation [28]:

$$D(\%) = \frac{C_t - C_o}{C_o} \times 100\% \quad (1)$$

where D(%) represents the decolorization rate of MO, C_t represents the MO concentration at time t min, and C_0 represents the initial MB concentration.

The photo catalytic reaction kinetics of all samples were calculated by the Langmuir–Hinshelwood (L–H) model as follows [29]:

$$-In\left(\frac{C_t}{C_o}\right) = k_{app}t \quad (2)$$

where k_{app} represents the apparent pseudo-first-order reaction rate constant (min^{-1}), and t represents the reaction time (min).

3. Results and discussion

3.1. Morphology and structure

The morphology and micro structure of the as-prepared chitosan membrane and Ag_3PO_4/chitosan membrane composites were characterized directly via SEM. As shown in Fig. 2a, a porous structure can be seen on the surface of the chitosan membrane; the sizes of micro-holes were roughly 10 um. From the SEM image of composite-1 (Fig. 2b), Ag_3PO_4 particles measuring about 200 nm were dispersed on the surface of the chitosan membrane with slight agglomeration. As the concentrations of the $AgNO_3$ solution continued to increase, the composite-2 exhibited many Ag_3PO_4 particles growing on the chitosan membrane (Fig. 2c). Compared with composite-1 and composite-2, composite-3 showed more Ag_3PO_4 particles on the chitosan membrane and attached densely in agglomerated forms. Clearly, Ag_3PO_4 particles were unevenly distributed on the chitosan membrane.

FTIR spectra of the chitosan membrane, pure Ag_3PO_4, and Ag_3PO_4/chitosan membrane composites are presented in Fig. 3. In FTIR spectra of the chitosan membrane, bands around 3340 cm^{-1} and 2877 cm^{-1} could be assigned to the amino (-NH_2) as well as hydroxyl (-OH) groups; the peaks at 1651 cm^{-1} and 1591 cm^{-1} were assigned to vibrations of the amide I band and amide II band, respectively [30]; and the characteristic absorption band at 1421 cm^{-1} corresponded to bending vibration of the -OH group. The two absorbent bands at 3440 cc and 1640 cm^{-1} in Ag_3PO_4 FTIR spectra were attributed to stretching and bending vibrations of OH of water molecules absorbed by Ag_3PO_4 [31].

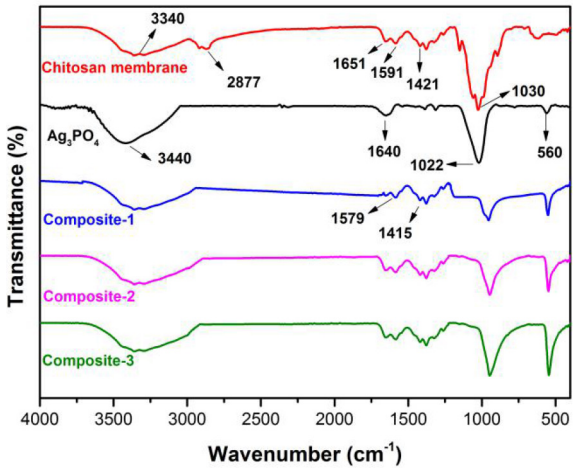

Fig. 3. FTIR spectra of chitosan membrane, pure Ag_3PO_4, composite-1, composite-2, and composite-3.

Moreover, Ag_3PO_4 exhibited other characteristic bands at 1022 cm^{-1} and 560 cm^{-1}, attributed to P-O groups. The peak at 560 cm^{-1} corresponded to the P-O bond vibration of PO_4^{3-} in the FTIR spectra of Ag_3PO_4/chitosan membrane composites, demonstrating that Ag_3PO_4 particles were successfully formed in situ in Ag_3PO_4/chitosan membrane composites. In addition, the band strength at 560 cm^{-1} of Ag_3PO_4/chitosan membrane composites increased as the concentration of the $AgNO_3$ solutions increased, indicating that the

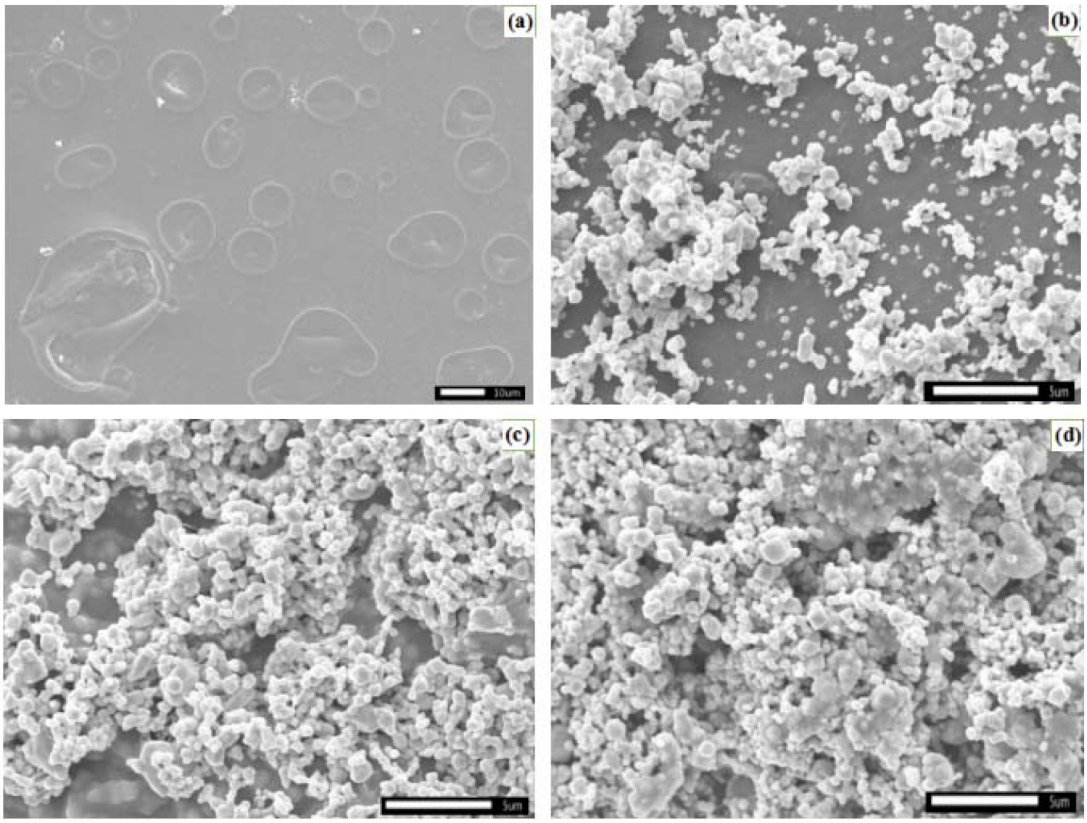

Fig. 2. SEM images of (a) chitosan membrane, (b) composite-1, (c) composite-2, and (d) composite-3.

content of Ag_3PO_4 on the surface of the chitosan membrane increased constantly. Furthermore, the bands of O-H and -NH_2 at 1421 cm^{-1} and 1591 cm^{-1} shifted to 1415 cm^{-1} and 1579 cm^{-1}, respectively, implying chelation of Ag^+ ions by the hydroxyl and amino groups of chitosan [32].

Fig. 4 displays the XRD spectrum of the as-synthesized chitosan membrane, pure Ag_3PO_4, and Ag_3PO_4/chitosan membrane composites. In the XRD pattern of the chitosan membrane, a main peak appeared at 2θ = 20.08°. In the Ag_3PO_4 diffraction patterns, eleven clear peaks emerged at 20.9°, 29.72°, 33.32°, 36.56°, 42.52°, 47.82°, 52.68°, 55.1°, 57.26°, 61.64°, and 71.92°, corresponding to the (110), (200), (210), (211), (220), (310), (222), (320), (321), (400), and (421) crystal planes of Ag_3PO_4 (JCPDS Card NO.06-0505), respectively [33]. In addition, Ag_3PO_4/chitosan membrane composites showed characteristic peaks of Ag_3PO_4, indicating that Ag_3PO_4 particles were successfully formed in situ on the surface of the chitosan membrane. No obvious characteristic peak of chitosan membrane appeared in the XRD pattern of Ag_3PO_4/chitosan membrane composites due to the low content or weak intensity of chitosan [32].

Chemical states of elements on the surface of composite-2 were further investigated by XPS. Fig. 5a shows the wide scan spectrum of composite-2, confirming the existence of C, Ag, P, and O elements in the sample. C1s peaks at 288.90 eV and 285.75 eV in Fig. 5b were assigned to C=O and C-OH bonds, respectively. The peak at 284.90 eV corresponded to C-C bonding in the chitosan membrane. As shown in Fig. 5c, peaks centered at 374.10 eV ($Ag3d_{3/2}$) and 368.05 eV ($Ag3d_{5/2}$) in the Ag3d spectrum revealed the presence of Ag^+ in composite-2. Fig. 5d presents the regional spectrum of P2p, where a peak at 133.40 eV corresponded to P^{5+} [34]. In Fig. 5e, the O1s spectrum can be found at 533.20 eV and 532.00 eV, composed of P-O of Ag_3PO_4 and HO from Ag_3PO_4 along with the chitosan membrane [35].

The optical absorption properties of photo catalysts is important in determining their photo catalytic activities; hence, the light absorbance behaviors of pure Ag_3PO_4 and Ag_3PO_4/chitosan membrane composites were investigated, with UV-vis diffuse reflectance spectra depicted in Fig. 6. Results indicate that the absorption edge of Ag_3PO_4 powder was around 530 nm, corresponding to the band gap of 2.3 eV, which is identical to the previous literature [36]. Additionally, the optical absorption of composite samples was much stronger and more durable than pure Ag_3PO_4 in the range of 500–800 nm, indicating that the visible light absorption properties of Ag_3PO_4/chitosan membrane composites could be greatly enhanced in the visible light region.

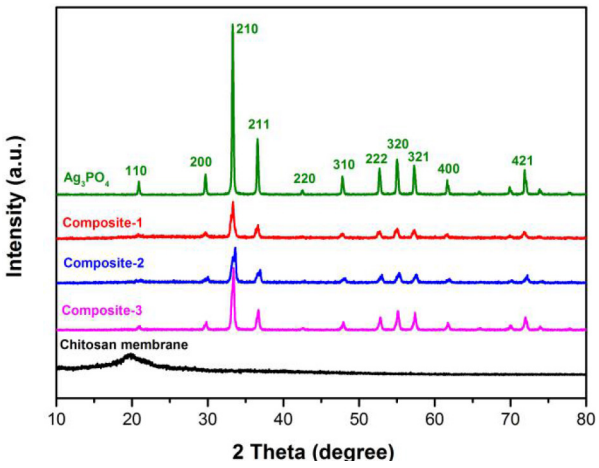

Fig. 4. XRD patterns of pure Ag_3PO_4, chitosan membrane, composite-1, composite-2, and composite-3.

3.2. Photo catalytic activity

To investigate the photo catalytic performance of as-prepared samples, a stable negatively charged organic pollutant MO solution was irradiated under visible light with different samples. Fig. 7a shows MO decolorization rates of the chitosan membrane, pure Ag_3PO_4, Ag_3PO_4 without light irradiation, only light irradiation and Ag_3PO_4/chitosan membrane composites. The color of the MO solution was only slightly lightened by the chitosan membrane, and pure Ag_3PO_4 exhibited relatively poor photo catalytic activity. Ag_3PO_4 without light irradiation and only light irradiation can hardly change the color of the MO. Composite-2 demonstrated optimal activity with a decolorization rate of nearly 90.1% after 40 min of visible light irradiation, whereas that of composite-1 and composite-3 was approximately 82.1% and 76.4%, respectively. The photo catalytic activity of composite-3 was less than that of composite-2 due to higher aggregation. Fig. 7b shows UV–vis spectral changes in the MO aqueous solution over composite-2 under visible light for different times. The intensity of the maximum absorption peak of MO at 464 nm reduced gradually with increasing irradiation time and nearly disappeared after 40 min. Fig. 7c displays the pseudo-first-order kinetics curves and reaction rate constant values (k_{app}) obtained from the slopes (Fig. 7d). The values of the chitosan membrane, pure Ag_3PO_4, composite-1, composite-2, and composite-3 were approximately 0.0032, 0.0129, 0.0449, 0.0517, and 0.0344, respectively. Findings suggest that the immobilization of Ag_3PO_4 on the surface of the chitosan membrane can promote photo catalytic activity in Ag_3PO_4.

The re-usability and stability of composite-2 was examined by recycling it under the same conditions. As shown in Fig. 8, the decolorization rate of composite-2 was roughly 55.5% after three recycling rounds. A reduction in the decolorization rate was likely due to photo corrosion of the Ag_3PO_4 particles.

Based on the above mentioned results, a possible photo catalytic mechanism of the Ag_3PO_4/chitosan membrane composites is elucidated in Fig. 9. Under visible light irradiation, Ag_3PO_4 was easily excited; many kinds of photo generated electrons (e^-) in its valence band excited to its conduction band, leaving generated holes (h^+) behind the valence band of Ag_3PO_4. As a result, electrons on the conduction band of Ag_3PO_4 reacted with O_2 dissolving in the solution to yield $^{\bullet}O_2^-$, which further reacted with H^+ to produce H_2O_2. Photo generated holes (h^+) in the valence band of Ag_3PO_4 reacted with OH^-/H_2O molecules and oxidated the MO solution to H_2O, CO_2, or other products [37].

4. Conclusions

I successfully prepared Ag_3PO_4/chitosan membrane composites via a facial method of in-situ synthesis. Com-

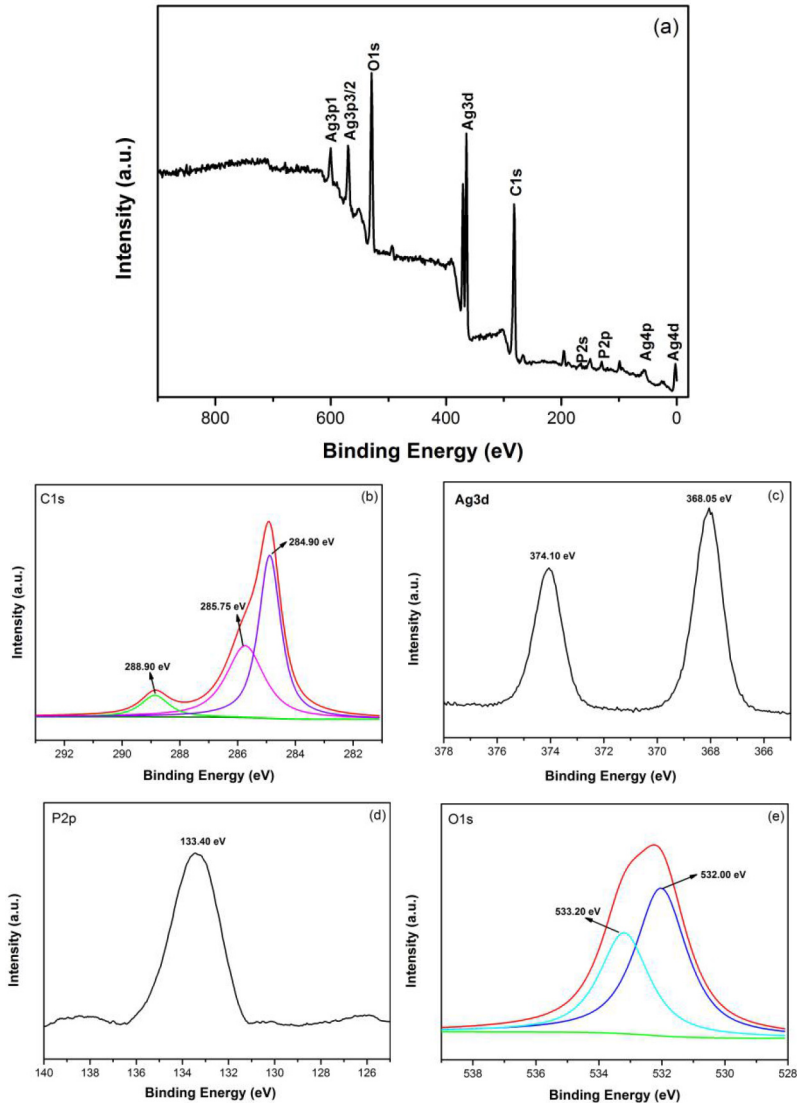

Fig. 5. XPS spectra of composite-2. (a) Fully scanned spectrum, (b) C1s, (c) Ag3d, (d) P2p, and (e) O1s.

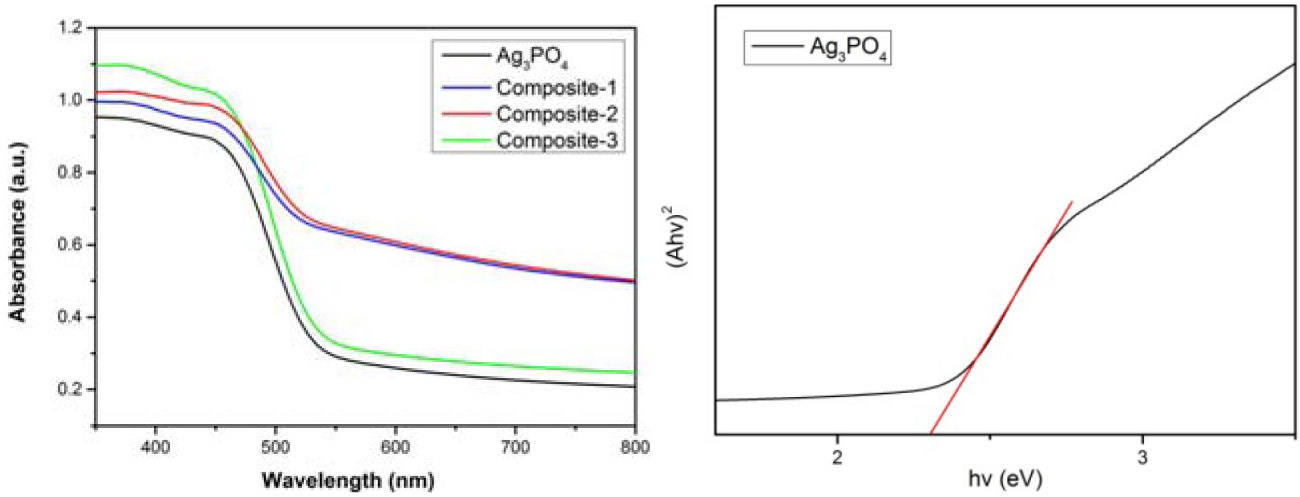

Fig. 6. UV-visible absorption spectra of pure Ag_3PO_4, composite-1, composite-2, composite-3 and the band gap of Ag_3PO_4.

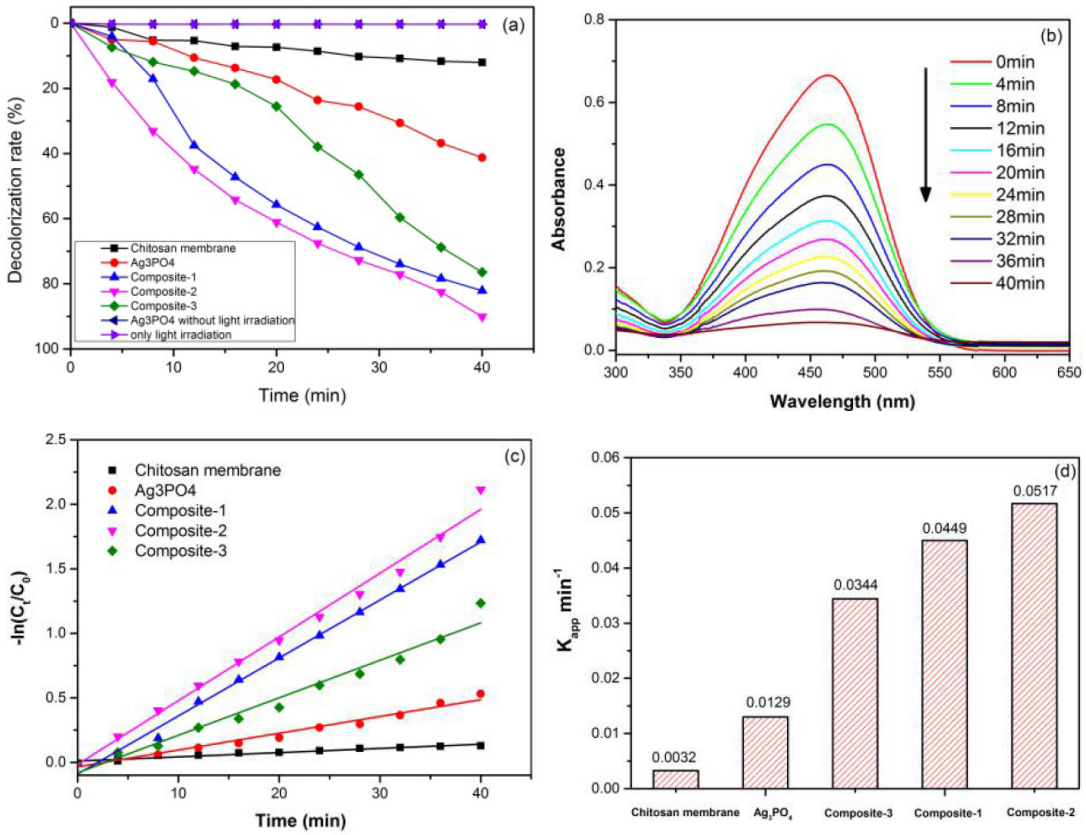

Fig. 7 (a) Photo catalytic decolorization rate of chitosan membrane, pure Ag_3PO_4, Ag_3PO_4 without light irradiation, only light irradiation and Ag_3PO_4/chitosan membrane composites. (b) UV–vis absorption spectra of MO solution using composite-2. (c) Photo catalytic kinetics of chitosan membrane, pure Ag_3PO_4, and Ag_3PO_4/chitosan membrane composites. (d) Apparent rate constant for decolorization of MO with different samples.

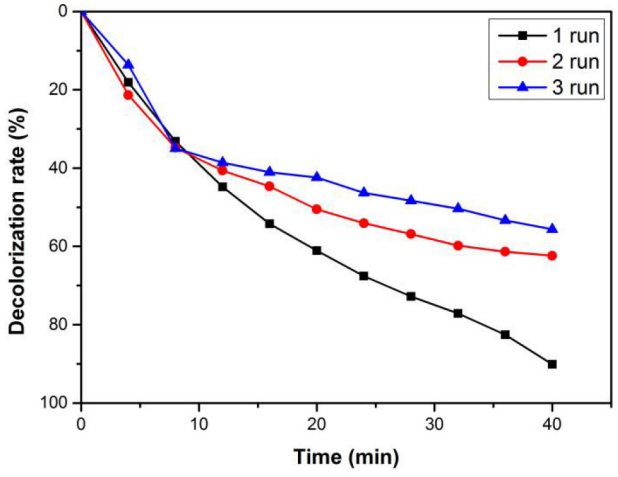

Fig. 8 Recyclability of composite-2 in photo degradation of MO under visible light irradiation.

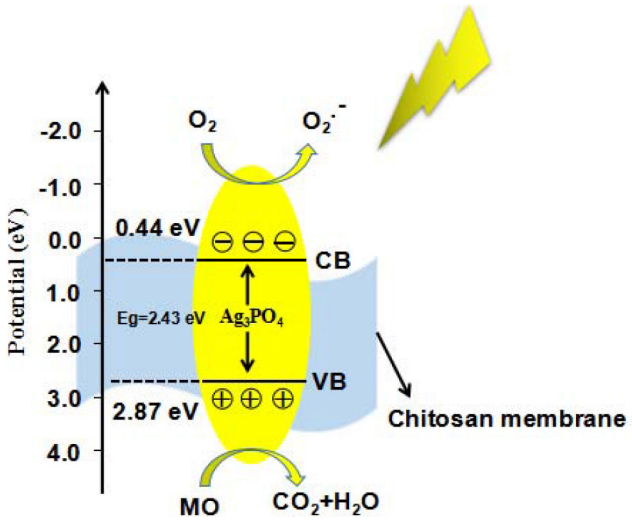

Fig. 9. Photo catalytic degradation mechanism of MO over Ag_3PO_4/chitosan membrane composites.

pared with pure Ag_3PO_4 powder, the composites exhibited better photo catalytic activity. Given many more Ag_3PO_4 particles and slighter aggregation, composite-2 presented the highest photo catalytic activity to degrade MO under visible light irradiation. The MO solution decolorization rate could reach 90.1% in 40 min under visible light irradiation. Consequently, this study presents a facile, green, low-cost way to prepare Ag_3PO_4/chitosan membrane composite photo catalysts with potential applications in wastewater treatment.

References

[1] Q. Wang, J.P. Ju, Y.Q. Tan, L.Y. Hao, Y.L. Ma, Y. Wu, H.W. Zhang, Y.Z. Xia, K.Y. Sui, Controlled synthesis of sodium alginate electro spun nanofiber membranes for multi-occasion adsorption and separation of methylene blue, Carbohyd. Polym., 205 (2019) 125–134.

[2] Y.L. Ma, P.F. Qi, J.P. Ju, Q. Wang, L.Y. Hao, R. Wang, K.Y. Sui, Y.Q. Tan, Gelatin/alginate composite nanofiber membranes for effective and even adsorption of cationic dyes, Compos. Part. B-Eng., 162 (2019) 671–677.

[3] Z.H. Guan, Y.Q. Wu, P. Wang, Q.Q. Zhang, Z.Y. Wang, Z.K. Zheng, Y.Y. Liu, Y. Dai, M.H. Whangbo, B.B. Huang, Perovskite photo catalyst $CsPbBr_{3-x}I_x$ with a band gap funnel structure for H_2 evolution under visible light, Appl. Catal. B-Environ., 245 (2019) 522–527.

[4] X.Z. Liang, P. Wang, M.M. Li, Q.Q. Zhang, Z.Y. Wang, Y. Dai, X. Y. Zhang, Y.Y. Liu, M.H. Whangbo, B.B. Huang, Adsorption of gaseous ethylene via induced polarization on plasmonic photo catalyst $Ag/AgCl/TiO_2$ and subsequent photo degradation, Appl. Catal. B-Environ., 220 (2018) 356–361.

[5] X.Z. Liang, P. Wang, B.B. Huang, Q.Q. Zhang, Z.Y. Wang, Y.Y. Liu, Z.K. Zheng, X.Y. Qin, X.Y. Zhang, Y. Dai, Ag_2ZnSnS_4/Mo-mesh photo electrode prepared by electroplating for efficient photo electrochemical hydrogen generation, J. Mater. Chem. A., 7 (2019) 1647–1657.

[6] X.L. Zhu, X.Z. Liang, P. Wang, Y. Dai, B.B. Huang, Porous Ag-ZnO micro spheres as efficient photo catalyst for methane and ethylene oxidation: Insight into the role of Ag particles, Appl. Surf. Sci., 456 (2018) 493–500.

[7] P. Wang, B.B. Huang, X.Y. Qin, X.Y. Zhang, Y. Dai, J.Y. Wei, M. H. Whangbo, Ag@AgCl: a highly efficient and stable photo catalyst active under visible light, Cheminform., 47 (2008) 7943.

[8] Y.Q. Yang, G.K. Zhang, Preparation and photo catalytic properties of visible light driven AgAgBr/attapulgite nanocomposite, Appl. Clay. Sci., 67–68 (2012) 11–17.

[9] G.P. Dai, J.G. Yu, G. Liu. A new approach for photo corrosion inhibition of Ag_2CO_3 photo catalyst with highly visible-light-responsive reactivity, J. Phys. Chem. C., 116 (2012) 15519–15524.

[10] X.C. Ma, Y. Dai, M. Guo, B.B. Huang, The role of effective mass of carrier in the photo catalytic behavior of silver halide-based Ag@AgX (X=Cl, Br, I): A theoretical study, Chem. Phys. Chem., 13 (2012) 2304–2309.

[11] Z.G. Yi, J.H. Ye, N. Kikugawa, T. Kako, S.X. Ouyang, H. Stuart-Williams, H. Yang, J.Y. Cao, W.J. Luo, Z.S. Li, Y. Liu, R.L. Withers, An orthophosphate semiconductor with photo oxidation properties under visible-light irradiation, Nat. Mater., 9 (2010) 559–564.

[12] M. Ge, N. Zhu, Y.P. Zhao, J. Li, L. Liu, Sunlight-assisted degradation of dye pollutants in Ag_3PO_4 suspension, Ind. Eng. Chem. Res., 51 (2012) 5167–5173.

[13] X.F. Yang, H.Y. Cui, Y. Li, J.L. Qin, R.X. Zhang, H. Tang, Fabrication of Ag_3PO_4-graphene composites with highly efficient and stable visible light photo catalytic performance, Acs. Catal., 3 (2013) 363–369.

[14] Z.M. Yang, G.F. Huang, W.Q. Huang, J.M. Wei, X.G. Yan, Y.Y. Liu, C. Jiao, Z. Wan, A.L. Pan, Novel Ag_3PO_4/CeO_2 composite with high efficiency and stability for photo catalytic applications, J. Mater. Chem. A., 2 (2013) 1750–1756 .

[15] M. Ge, M.M. Tan, G.H. Cui. Synthesis of $Ag_3PO_4/BiVO_4$ Composite photo catalyst and its photo catalytic degradation of dyes under visible light irradiation, Acta Phys-Chim Sin., 30 (2014) 2107–2112.

[16] S.Y. Zhu, D. Xu, S. Fang, Z. Geng, X. Yang, Sunlight-responsive Ag_2S/Ag_3PO_4 composite preparation and degradation of salicylic acid, Chem. J. Chinese. U., 35 (2014) 1286–1292.

[17] G. Gyawali, S.W. Lee, Microwave hydrothermal synthesis and characterization of Ag_3PO_4/MoS_2 composite photo catalyst, J. Nanosci., 16 (2016) 11158–11163 .

[18] J. Liu, Q.Y. Tian, Z.H. Wu, Synthesis and photo catalytic application of trinary structural $g\text{-}C_3N_4/Ag/Ag_3PO_4$ composite nanomaterials, J. Environ. Chem. Eng., 5 (2017) 5777–5785.

[19] G. Panthi, S.J. Park, S.H. Chae, T.W. Kim, H.J. Chung, S.T. Hong, M. Park, H.Y. Kim, Immobilization of Ag_3PO_4 nanoparticles on electro spun PAN nanofibers via surface oximation: Bifunctional composite membrane with enhanced photo catalytic and antimicrobial activities, J. Ind. Eng. Chem., 45 (2017) 277–286.

[20] P. Wang, C.C. He, L.Q. Hu, S.H. Chen, X.Z. Yin, J. Xu, L.X. Wang, H. Wang, Load of Ag_3PO_4 particles on sulfonated polyphenylene sulfide superfine fibre with high visible-light photo catalytic activity, Fiber. Polym., 19 (2018) 1379–1385.

[21] Q.Y. Wang, J. Cai, L.N. Zhang, In situ synthesis of Ag_3PO_4/cellulose nanocomposites with photo catalytic activities under sunlight, Cellulose, 21 (2014) 3371–3382.

[22] K.E. Crompton, J.D. Goud, R.V. Bellamkonda, T.R. Gengenbach, D.I. Finkelstein, M.K. Horne, J.S. Forsythe, Polylysine-functionalised thermoresponsive chitosan hydro gel for neural tissue engineering, Biomaterials, 28 (2007) 441–449.

[23] A.A. Sarhan, D.M. Ayad, D.S. Badawy, M. Monier, Phase transfer catalyzed heterogeneous N-deacetylation of chitin in alkaline solution, React. Funct. Polym., 69 (2009) 358–363.

[24] Y. Kawamura, M. Mitsuhashi, H. Tanibe, H. Yoshida, Adsorption of metal ions on polyaminated highly porous chitosan chelating resin, Ind. Eng. Chem. Res., 32 (1993) 386–391.

[25] L.L. Fan, C.N. Luo, Z. Lv, F.G. Lu, H.M. Qiu, Removal of Ag^+ from water environment using a novel magnetic thiourea-chitosan imprinted Ag^+, J. Hazard. Mater., 194 (2011) 193–201.

[26] D. Harikishore, K. Reddy, S.M. Lee. Application of magnetic chitosan composites for the removal of toxic metal and dyes from aqueous solutions, Adv. Colloid. Interfac., 201–202 (2013) 68–93.

[27] R.S. Vieira, M.M. Beppu. Dynamic and static adsorption and desorption of Hg(II) ions on chitosan membranes and spheres, Water. Res., 40 (2006) 1726–1734.

[28] C.L. Yu, L.F. Wei, W.Q. Zhou, J.C. Chen, Q.Z. Fan, H. Liu, Enhancement of the visible light activity and stability of Ag_2CO_3 by formation of AgI/Ag_2CO_3 heterojunction, Appl. Surf. Sci., 319 (2014) 312–318.

[29] C.H. Cao, L. Xiao, L. Liu, H.Y. Zhu, C.H. Chen, L. Gao, Visible-light photo catalytic decolorization of reactive brilliant red X-3B on Cu_2O/cross linked-chitosan nanocomposites prepared via one step process, Appl. Surf. Sci., 271 (2013) 105–112.

[30] X.C. Liang, J.J. Duan, Q. Xu, X.Q. Wei, A. Lu, L.N. Zhang, Ampholytic microspheres constructed from chitosan and carrageenan in alkali/urea aqueous solution for purification of various wastewater, Chem. Eng. J., 317 (2017) 766–776.

[31] P.Y. Dong, Y.H. Wang, B.C. Cao, S.Y. Xin, L.N. Guo, J. Zhang, F. H. Li, Ag_3PO_4 /reduced graphite oxide sheets nanocomposites with highly enhanced visible light photo catalytic activity and stability, Appl. Catal. B. Environ., 132–133 (2013) 45–53.

[32] Q.H. Cao, L. Xiao, J. Li, C.H. Cao, S. Li, J. Wang, Morphology-controlled fabrication of Ag_3PO_4 /chitosan nanocomposites with enhanced visible-light photo catalytic performance using different molecular weight chitosan, Powder. Technol., 292 (2016) 186–194.

[33] H. Xu, H.Z. Zhao, Y.H. Song, W. Yan, Y.G. Xu, H.P. Li, L.Y. Huang, S. Yin, Y.P. Li, Q. Zhang, H.M. Li, $g\text{-}C_3N_4$ /Ag_3PO_4 composites with synergistic effect for increased photo catalytic activity under the visible light irradiation, Mat. Sci. Semicon. Proc., 39 (2015) 726–734.

[34] X.F. Yang, Z.P. Chen, J.S. Xu, H. Tang, K.M. Chen, Y. Jiang, Tuning the morphology of $g\text{-}C_3N_4$ for improvement of Z-scheme photo catalytic water oxidation, Acs. Appl. Mater. Inter., 7 (2015) 15285.

[35] C.M. Fan, Y.F. Wang, Y.W. Wang, C.M. Fan, Synthesis, Regeneration and photo catalytic activity under visible-light irradiation of $Ag/Ag_3PO_4/g\text{-}C_3N_4$ hybrid photo catalysts, Acta, Phys-Chim. Sin., 30 (2014) 729–737.

[36] T.H. Zhou, C.Z. Zhang, H. Yang, H.W. Zhang, R.N. Suo, Y.S. Xie, G. Liu, Fabrication of $Ag_3PO_4/GO/NiFe_2O_4$ composites with highly efficient and stable visible-light-driven photo catalytic degradation of rhodamine B, RSC. Adv., 8 (2018) 28179–28188 .

[37] G.D. Chen, M. Sun, Q. Wei, Y.F. Zhang, B.C. Zhu, B. Du, Ag_3PO_4/graphene-oxide composite with remarkably enhanced visible-light-driven photo catalytic activity toward dyes in water, J. Hazard. Mater., 244–245 (2013) 86–93.